8/10/81 M.S. (1)

B6326

JULY 1981

PPPL-1819
UC-20F

JF-2424

MASTER

ION BERNSTEIN-WAVE EXCITATION VIA FINITE-LARMOR-RADIUS MODE-TRANSFORMATION PROCESS

BY

M. ONO, K.L. WONG AND G.A. WURDEN

PLASMA PHYSICS LABORATORY

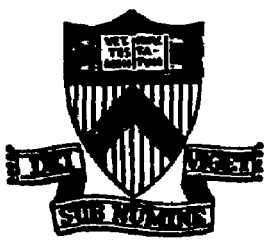

DISTRIBUTION OF THIS DOCUMENT IS UNLIMITED

PRINCETON UNIVERSITY
PRINCETON, NEW JERSEY

This work was supported by the U.S. Department of Energy Contract No. DE-AC02-76-CHO 3073. Reproduction, translation, publication, use and disposal, in whole or in part, by or for the United States government is permitted.

Ion Bernstein-Wave Excitation Via Finite-Larmor-Radius Mode-Transformation Process

M. Ono, K. L. Wong, and G. A. Wurden

Plasma Physics Laboratory, Princeton University
Princeton, New Jersey 08544

ABSTRACT

Ion Bernstein wave excitation and propagation via finite-Larmor-radius mode transformation have been investigated. It is shown that in the ion cyclotron range of frequency $\omega \lesssim 2\Omega_i$, the finite-Larmor-radius effect removes the wave singularity at the lower-hybrid resonance layer, enabling an externally initiated electron plasma wave to propagate freely through the resonance layer, transforming continuously into an ion Bernstein wave. In an ACT-1 hydrogen plasma ($T_e \simeq 2.5$ eV, $T_i \simeq 1.5$ eV), linear excitation of ion Bernstein waves has been investigated experimentally for $\omega \lesssim 2\Omega_i$. The mode-transformation process resulting in a strong $\omega \simeq 2\Omega_i$ ion Bernstein wave excitation without observable reflections has been experimentally verified. Detailed measurements of wave dispersion relation and of the wave-packet trajectory show excellent agreement with theory. The relevancy of the present work to fusion plasmas will be also discussed.

DISCLAIMER

[redacted]

DISTRIBUTION OF THIS DOCUMENT IS UNLIMITED

I. Introduction

Application of radiofrequency (rf) power near the ion cyclotron range of frequency and also near the lower-hybrid frequency offers a promising outlook for heating fusion plasmas to ignition temperatures. In this frequency range, the radiofrequency (or microwave) power is readily available and relatively inexpensive. One of the most intensely investigated radiofrequency heating phenomena in recent years is the mode-conversion (transformation) process, arising from the finite-ion-Larmor-radius effect near the cold plasma resonances.[1-6] This process can modify the cold plasma wave dispersion relation near the resonances and can profoundly affect the overall rf heating efficiencies. As the heating regimes move closer to hotter and denser reactor-like plasmas, the finite-ion-Larmor-radius effect is expected to assume increasingly important roles in determining the physics of the heating waves.

Recently, it was also proposed that a waveguide-launched ion Bernstein wave ($\omega \approx 2\Omega_i$) may offer an attractive alternative method for heating fusion plasmas to ignition temperatures.[7,8] Theoretical work on waveguide-coupling and ray-tracing suggests a promising prospect for heating fusion plasmas to ignition temperatures by relatively simple waveguide couplers.[8,9] Preliminary experimental results on ion Bernstein wave excitation and mode-transformation process has recently been reported.[10] In this paper we present a more detailed

account of our work including relevant theoretical analysis as well as discussion on implications of the present work. The plan for this paper is as follows:

In Sec. II, we derive relevant dispersion relations and describe the physics of mode-transformation process in some detail. The emphasis will be placed on the theory related to the ACT-1 experiments. In Sec. IIIA, we describe the overall aspects of the ACT-1 device and experimental set-up. In Sec. IIIB, we describe a technique to measure the hydrogen ion concentrations. In Sec. IV, we present experimental data on the ion Bernstein wave excitation and propagation. Finally, in Sec. V, we conclude with summary and discussion.

II. Theory of Ion Bernstein Wave Excitation

The relevant electrostatic wave dispersion relation for $\omega = \mathcal{O}(\Omega_i)$ can be expressed as[11]

$$k_\perp^2 K_{xx} + k_\parallel^2 K_{zz} = 0 \qquad (1)$$

where

$$K_{xx} = 1 + \sum_\sigma \omega_{p\sigma}^2 \frac{\exp(-\lambda_\sigma)}{\lambda_\sigma} \sum_{n=1}^{\infty} \frac{I_n(\lambda_\sigma) 2n^2}{(n^2\Omega_\sigma^2 - \omega^2)}$$

and

$$K_{zz} = 1 + 2 \frac{\omega_{pe}^2}{\omega^2} y^2 [1 + yZ(y)] \simeq - \frac{\omega_{pe}^2}{\omega^2} .$$

Here, $\lambda_\sigma \equiv k_\perp^2 T_\sigma/m_\sigma\Omega_\sigma^2$, σ designates all species, I_n is the modified Bessel function, $y \equiv (\omega/k_\parallel)\sqrt{m_e/2T_e}$, and Z is the plasma dispersion function.

In order to illuminate the physics of mode-transformation, it is instructive to expand terms in Eq. (1) for small λ_σ which is a good approximation for $\omega \lesssim 2\Omega_i$ excitation. To a leading order in λ_σ Eq. (1) takes on the following form:

$$1 - \frac{k_\perp^2}{k^2} \sum_i \frac{\omega_{pi}^2}{\omega^2-\Omega_\sigma^2} + \frac{k_\perp^4}{k^2} \sum_i \frac{3\omega_{pi}^2 (T_i/m_i)}{(4\Omega_i^2-\omega^2)(\omega^2-\Omega_i^2)} - \frac{k_\parallel^2}{k^2} \frac{\omega_{pe}^2}{\omega^2} = 0 \qquad (2)$$

where we have assumed cold electrons (i.e., $\omega/k_\parallel >> V_{Te}$) and neglected the electron terms in K_{xx} since $\omega_{pe}^2/\Omega_e^2 << \omega_{pi}^2/\omega^2 \simeq \omega_{pi}^2/\Omega_i^2$. Equation (2) is a quadratic equation in $k_\perp^2$ which can be expressed as

$$a\, k_\perp^4 + b\, k_\perp^2 - c = 0 \qquad (3)$$

where

$$a = \sum_i \frac{3\omega_{pi}^2 (T_i/m_i)}{(4\Omega_i^2-\omega^2)(\omega^2-\Omega_i^2)}$$

$$b = 1 - \sum_i \frac{\omega_{pi}^2}{\omega^2-\Omega_i^2}$$

$$c = -k_\parallel^2 \left(1 - \frac{\omega_{pe}^2}{\omega^2}\right) \simeq +k_\parallel^2 \frac{\omega_{pe}^2}{\omega^2} \,.$$

The coefficients a, b, and c represent the finite-Larmor-radius (thermal) correction, the cold ion, and the cold electron terms, respectively. Trivially, the solution of Eq. (3) is written as

$$k_\perp^2 = \frac{-b \pm \sqrt{b^2+4ac}}{2a} \quad . \tag{4}$$

The cold plasma (or lower-hybrid) resonance occurs when b vanishes near $\omega \simeq \omega_{pi}$. We shall now consider the evolution of the wave introduced at the low density plasma edge ($b \simeq 1$) as it propagates toward the lower-hybrid resonance layer ($b \simeq 0$).

For the present case where $\Omega_i < \omega \lesssim 2\Omega_i$, the coefficient"a" is positive and the propagating root of Eq. (4) can be written as

$$k_\perp^2 = \frac{-b + \sqrt{b^2+4ac}}{2a} \quad . \tag{5}$$

The behavior of Eq. (5) is shown in Fig. 1 as a solid curve. In a low density region $b \simeq 1 >> \sqrt{4ac}$, the wave is an electron plasma wave (EPW) and Eq. (5) can be approximated as

$$k_\perp^2 \simeq \frac{c}{b} \simeq \frac{\omega_{pe}^2}{\omega^2} k_\parallel^2 \quad . \tag{6}$$

As the wave approaches the resonance so that $b \simeq 0 << \sqrt{4ac}$, electron plasma wave changes over to a wave with the following dispersion relation:

$$k_\perp^2 \simeq \sqrt{\frac{|c|}{a}} \simeq \sqrt{\left(\frac{m_i}{m_e}\right)\left(\frac{k_\perp^2}{k_\parallel^2}\right)} \sqrt{\frac{(4\Omega_i^2-\omega^2)(\omega^2-\Omega_i^2)}{3\omega^2 v_i^2 k_\perp^2}} \quad . \qquad (7)$$

This wave can exist for b = 0 because of the ion thermal term, and therefore, we call this intermediate mode, the lower hybrid thermal wave (LHTW). As the wave propagates passed the resonance layer into higher density region so that $\omega_{pi}^2 >> \omega^2$, $k_\perp^2$ becomes sufficiently large thereby making the ion terms to dominate over the electron term ($|b|^2 > 4ac$). In this region, the wave is an ion Bernstein wave whose approximate dispersion relation can be obtained from Eq. (5) to be

$$k_\perp^2 \simeq \frac{|b|}{a} \simeq \sum_i \frac{\omega_{pi}^2}{\omega^2-\Omega_i^2} \Big/ \sum_i \frac{3\omega_{pi}^2 (T_i/m_i)}{(4\Omega_i^2-\omega^2)(\omega^2-\Omega_i^2)} \quad . \qquad (8)$$

As can be seen from Fig. 1, an externally launched electron plasma wave connects smoothly onto the ion Bernstein wave via a lower-hybrid thermal wave. Propagating further into the plasma toward higher magnetic field region causes $k_\perp \rho_i$ to increase and requires the inclusion of the higher order terms in Eq. (1) which then can be solved numerically.

In analyzing the above mode-transformation process, we have used a uniform plasma theory which requires the WKB approximation (i.e., $\partial k_\perp / \partial r \; k_\perp^{-2} << 1$) to be satisfied in the mode-transformation region ($b \simeq 0$). Using Eq. (7) one can obtain the following inequality for the WKB condition:

$$\frac{\partial k_\perp}{\partial x}\frac{1}{k_\perp^2} \simeq \frac{1}{4k_\perp}\left[\frac{\partial T_i}{\partial x}\frac{1}{T_i}\right] \simeq \frac{\lambda_\perp}{8\pi L} << 1 \qquad (9)$$

where L is the ion temperature gradient scale length. It is interesting to note that in this region, due to the weak density dependence of the wave dispersion relation in Eq. (7), the important gradient scale length is that of the ion temperature. Since $\lambda_\perp$ is typically $\lesssim$ 1 cm and L is larger than 1 mm in almost any experimental situations, the WKB treatment of the present mode-transformation process is justified, and no wave reflection should occur.

As a comparison, we briefly consider the well-known lower hybrid heating case where $\omega >> \Omega_i$. In this case, the thermal coefficient "a" is negative and the propagating solutions only exist for $b > \sqrt{4|a|c}$. From Eq. (4), we obtain

$$k_\perp^2 = \frac{b \mp \sqrt{b^2-4|a|c}}{2|a|} \quad . \qquad (10)$$

The upper-root represents the initially launched electron plasma wave

$$k_\perp^2 = \frac{b-\sqrt{b^2-4|a|c}}{2|a|} \simeq \frac{c}{b} \simeq \frac{\omega_{pe}^2}{\omega^2} k_\parallel^2 \ , \qquad (11)$$

which then turns around when $b^2 = 4|a|c$ and mode-converts into the lower root, known as a hot-plasma wave[1]

$$k_\perp^2 = \frac{b+\sqrt{b^2-4|a|c}}{2|a|} \simeq \frac{b}{|a|} \quad . \tag{12}$$

In Fig. 1 we plot this conversion process with a dashed curve. Even though the mode-conversion picture shown in Fig. 1 is essentially correct, it should be emphasized that the present WKB treatment for the lower hybrid heating case breaks down near the turning point, and therefore requires a proper treatment of the wave differential equation.[1] Since this problem has been investigated in a number of lower-hybrid heating papers,[1,12,13] we refer the interested readers to these references.

In Fig. 2(a) we plot $k_\perp$ numerically calculated from Eq. (1) versus radial position, using typical ACT-1 parameters. The wave frequency has been chosen so that $\omega/\Omega_H \simeq 1.9$ at $x=0$. Density increases linearly with radial position, x, and when $x \simeq 2$ cm the cold-plasma lower-hybrid resonance condition, $b=0$ is satisfied. The dashed curve ($T_i=0$) shows propagation for $b>0$, then resonance ($k_\perp^2 \to \infty$) at $b=0$. The wave is evanescent ($k_\perp^2<0$) for $b<0$. The solid curve represents warm-ion case ($T_i = 1.5$ eV) showing continuous transformation from an electron plasma wave into an ion Bernstein wave. In Fig. 1(b) the corresponding wave trajectories are shown. As expected for the warm-ion case, the mode-

transformation process leads to continuous inward propagation of the wave through the cold plasma resonance.

Before going on to the experiment, we briefly describe various properties of ion Bernstein wave[14] which are relevant to the experiment. The ion Bernstein wave, like electron plasma wave, is a backward propagating wave where $\vec{V}_{g_\perp}$ is anti-parallel to $\vec{V}_{ph_\perp}$. The wave energy (group velocity direction) flows obliquely to the magnetic field [see Fig. 2(b)], but with angle $\theta \propto V_{Ti}\lambda_\parallel$ which is quite different from the electron plasma wave where $\theta \propto n_e^{-1/2}$. The dependence of θ with $\lambda_\parallel$ causes the wave packet to spread in radial direction, as opposed to the "resonance cone" behavior of the electron plasma wave.[15] The perpendicular wavelength of the ion Bernstein wave is determined mainly by the local ion temperature and magnetic field. From Eq. (1), one can write for a small electron term (i.e., $\lambda_\perp/\lambda_\parallel \sqrt{m_i/m_e} \ll 1$),

$$\frac{\omega}{K_\perp} = V_{Ti}\, g\left(N_i, \frac{\omega}{\Omega_i}\right) \tag{13}$$

where g is a function with argument N_i and ω/Ω_i. In a single ion species plasma, for $\omega \leq 2\Omega_i$, from Eq. (8) one obtains

$$\lambda_\perp \simeq V_{Ti} \quad f^{-1} \quad \sqrt{\frac{3}{4(\Omega_i/\omega)^2 - 1}} \tag{14}$$

where f is the wave frequency. Therefore, in a given magnetic field region, the ion Bernstein perpendicular wavelength is proportional to the ion thermal velocity.

III. Experimental Set-Up and Measurement Techniques

A. ACT-1 Research Torus

The experiments were performed in the Princeton ACT-1 research torus.[16] A schematic of the device is shown in Fig. 3. A steady-state pure toroidal magnetic field of up to 5.5 kG is generated by 26 sets of toroidal field coils with a field ripple along the minor axis of $\lesssim 0.5\%$. A set of two vertical field coils are installed to provide a small amount of vertical as well as horizontal correction field of $\lesssim 10$ G. The vacuum chamber consists of 26 identical wage-type sections forming a toroidal plasma bore of 59 cm major radius and 10 cm minor radius. Each chamber section contains a large 10 cm × 40 cm port to provide a good access to the plasma. The plasma is produced by a hot tungsten filament plasma source shown in Fig. 4 and the plasma diameter is usually limited to $\lesssim 15$ cm by a set of copper limiters. The filament is heated to thermionic emission temperatures, and the emitted electrons are accelerated by a bias voltage (typically 150 volts) applied between the filament and a grounded limiter, acting as an anode. The accelerated electrons circulate around the torus many times before being lost due to ∇B drift. A small vertical field can be also introduced to vary the rate of

the vertical drift. The relatively long electron path length (60-300 m) can provide efficient ionization of the background neutral gases. A good stable discharge can be maintained even as low a gauge neutral pressure of 7×10^{-6}Torr, leaving a warm-ion (~1.5 eV), highly ionized (≲50%), low collisionality hydrogen plasma with $n_e \lesssim 10^{11}$ cm^{-3}. As shown by Fig. 4, the plasma consists of a narrow vertical band of hot electron region near the filament and a diffused plasma region filling the space bounded by the limiter. Since the diffused plasma is free of hot electrons and is nearly Maxwellian, the wave propagation experiments are conducted in this region. Typical radial profiles of the plasma density and temperatures are shown in Fig. 5(a) and (b). The plasma density is measured by the lower hybrid resonance cone propagation technique and by Langmuir probe ion saturation current. The electron temperature is measured by a Langmuir probe and the ion temperature profile is obtained from the ion Bernstein wave dispersion relation which will be discussed in detail in Section IV. The plasma is found to be relatively uniform in the vertical direction. Relative ion concentrations are measured by the low-frequency resonance-cone propagation technique[17] which will be discussed in the next section.

In Fig. 3 a schematic of wave excitation and detection set-up is shown. Low level rf power (<0.1 watt) with alternate phase is applied to a pair of electrostatic antennas, which are placed one port apart (~16.5 cm) at the outer edge (low-field side) of the plasma, 1/8" to 1/4" behind the plasma limiter. This type of electrostatic antenna has been used previously to excite the electron plasma wave,[18,19] and also the cold electrostatic ion cyclotron wave.[17] In the present experiment, the excitation frequency was set at $f \simeq 2f_{ci}(H_1^+) \simeq$ 12-14 MHz, corresponding to $B_o \simeq$ 4.0-4.6 kG near the outer plasma edge, and the effective parallel wavelength of the antenna was put at $\lambda_{\parallel} \simeq 34$ cm so that $\omega/k_{\parallel} \simeq 4.0 \times 10^8$ cm/sec $>> (2\,T_e/m_e)^{1/2} \simeq 10^8$ cm/sec. The excited waves were detected by rf probes placed at various toroidal locations.

B. Ion Concentration Measurement

Various ion concentration measuring techniques have been investigated previously in Princeton's L-4 linear research device.[17,20] In particular, it was found that the low-frequency-resonance-cone provides a quick and non-perturbing way of measuring the local ion concentrations in the plasma.[17] The low-frequency-resonance-cone propagates below each ion cyclotron frequency with a propagation angle (with respect to the local magnetic field line) which depends

primarily on the ion concentrations. One can obtain the dispersion relation from Eq. (1) in the following form:

$$\theta^2 \frac{m_H}{m_e} = \sum_i \frac{N_i \omega^2 Z_i^2}{A_i\left(\Omega_i^2 - \omega^2\right)} \tag{15}$$

where $\theta = \tan^{-1}(V_{g_\perp}/V_{g_\parallel}) \simeq \tan^{-1}(k_\parallel/k_\perp)$, N_i is the ion concentrations, Z_i is the ion charge state, and A_i is the ion mass number. In deriving Eq. (10), we have assumed electrons to be cold (i.e., $\omega/k_\parallel > V_{Te}$) and the plasma density is sufficiently high so that $\omega_{pi} > \Omega_i$. A nice feature of Eq. (10) is that the concentration N_i depends only on the cone angle and the local magnetic field. For $\omega \sim \Omega_i$, one can in most cases neglect other ion terms and use the following approximate relation to determine N_i:

$$N_i \simeq \frac{A_i}{Z_i^2}\left(\frac{\Omega_i^2}{\omega^2} - 1\right) \frac{m_H}{m_e}\theta^2 \ . \tag{16}$$

Equation (16) is a convenient relation to obtain the first order ion concentration before proceeding on to the full solution of Eq. (15).

The resonance cone is excited by the same electrostatic antenna used for the ion Bernstein wave excitation as described in Sec. III (a). The excited resonance cone propagates obliquely to the magnetic field line in a well defined wave packet which is measured by radially scanning probes placed at various toroidal locations. In Fig. 6(a),

radial amplitude profiles of the resonance cone launched from the exciters placed 3 ports (top trace) and 6 ports (bottom trace) away from the probe. One should remember that the radially scanned probe intersects both the resonance cones propagating the "short" way and the "long" way around the torus. By measuring the wave packet displacement within a known toroidal distance ΔZ, one can obtain the cone angle $\psi = \tan^{-1}\Delta r/\Delta Z \approx \Delta r/\Delta Z$. In Fig. 6(b) we show the measured ψ as a function of ω/Ω_i in a typical hydrogen discharge plasma used in our experiment. We note that there are three propagating branches which corresponds to the presence of three ion-species in the plasma namely, H_1^+, H_2^+, and H_3^+. The relative ion concentrations in this case is 60% H_1^+, 16% H_2^+, and 24% H_3^+. In our hydrogen plasma, we observe H_1^+ to be a dominant ion-species. The ion concentrations are also found to be uniform in the experimental region, within our experimental uncertainty, $\delta N_i/N_i \approx 20\%$.

IV. Experimental Results

Figure 7 displays typical radial profiles of the excited ion Bernstein wave amplitude for various axial positions, Z. Here we have defined the radial position so that the wave launcher is located at x = 0. Inward propagation of the excited-wave packet is seen as it travels away from the antenna. The cold-plasma resonance, located at x = 1 cm, causes no visible perturbation to the wave trajectory. The wave packet however starts to spread after mode-transforming into ion Bernstein wave as expected from theory (see Sec. II). To identify the excited wave, we measured perpendicular and parallel wavelengths by interferometry and in Fig. 8(a) typical radial interferometer patterns are shown for several values of ω/Ω_H. The wave exhibits a cutoff ($\lambda_\perp \to \infty$) as ω approaches $2\Omega_H$, and $\lambda_\perp$ decreases with ω for given x. For given ω, the wavelength also decreases with increasing x (decreasing R) which reduces ω/Ω_H.

In Fig. 8(b), where the radial interferometer pattern is shown for various time delays of the boxcar sampler window, the wave phase front moves towards the antenna, confirming the backward-propagating nature of the ion Bernstein wave. In Fig. 8(c) we have plotted the measured wave dispersion relation (dots) at x = 4 cm and find excellent agreement with the theoretical curve for T_i = 1.5 eV. The

measured parallel wavelength, $\lambda_{\parallel} \approx 34$-$38$ cm, also agrees reasonably well with the effective antenna wavelength, $\lambda_{\parallel} \approx 34$ cm. From these measurements we conclude that the excited wave is indeed the ion Bernstein wave.

We recall that in the earlier Q-machine experiments on ion Bernstein wave,[21,22] it was critical to align the exciter exactly along the magnetic field line to observe the wave excitation. The main difficulty in the Q-machine experiment was in satisfying the cold electron condition, $\omega/k_{\parallel} \approx 2f_{ci}\lambda_{\parallel} > 3(T_e/m_e)^{1/2}$, to avoid strong electron Landau damping. In the experiment, $f_{ci} \approx 200$ kHz ($m_i \approx 40$) and $(T_e/m_e)^{1/2} \approx 2 \times 10^7$ cm/sec, which then gives the required $\lambda_{\parallel}$ to be larger than 150 cm, comparable to the machine length L ≈ 100 cm. In our experiment, this difficulty was minimized by using a hydrogen plasma, $f_{ci} \approx 6$ MHz and $(T_e/m_e)^{1/2} \approx 7 \times 10^7$ cm/sec, which gives the required $\lambda_{\parallel}$ to be only larger than 18 cm. Indeed, we find that the ion Bernstein wave is one of the most readily excitable waves with excellent coherence in our warm-ion hydrogen plasma.

Returning to Fig. 7, we have also drawn on this plot ion-Bernstein-wave trajectories calculated using experimental parameters. To account for the spread in $\lambda_{\parallel}$ due to the finiteness of the antenna, trajectories are shown for three values of $\lambda_{\parallel}$. This calculation agrees reasonably well with the observed wave trajectory and explains to some

extent the wave packet spreading. The amplitude modulation of the wave packet in Fig. 7 is apparently an interference phenomena caused by the interference of the ion Bernstein wave with the near field (electromagnetic) component of the antenna.[15]

By using a vertically movable, horizontally scanning probe, we have investigated the radial phase front of ion Bernstein wave. In this case, we have used a pair of two straight antennas 12 cm in height placed ~6 mm behind a set of straight limiters. In Fig. 9(a) we show radial interferometry patterns obtained at various vertical positions (as labeled). The wave coherence remains quite good even though the exciter, in this case, is placed 11 ports away (more than a third of way around the torus) from the probe. At this point, the wave packet has penetrated radially into the plasma and also has a large radial extent. By connecting the equivalent phase points on the interferometry patterns, one can obtain a radial wave phase front pattern as shown by Fig. 9(b). We observe a coherent phase pattern which retains the original exciter image even near the center of the plasma. The small curvature of the phase front can be attributed to the slightly weaker magnetic field in the upper right region. This type of phase pattern also shows that the vertical plasma variation is small in our plasma.

In ACT-1, by changing the neutral pressure, the hydrogen ion temperature can be varied over a wide range (1/40 eV to 2 eV), and Fig. 10(a) shows the interferometry output for several neutral pressures. For the high-pressure case ($p_H = 4 \times 10^{-4}$ Torr) the ions are essentially cold ($T_i \simeq 1/40$ eV) and the excited wave is the well-known electron plasma wave;[20] the electron plasma wave excited in this region behaves quite like the cold-ion case (dashed curves in Fig. 2) where the wave packet stays near the surface, outside the cold plasma resonance. Strictly speaking, even at $T_i \simeq 1/40$ eV, the mode-transformation should eventually occur into a very short, submillimeter ion Bernstein wave. However, at such short wavelength, the probe is no longer sensitive and the wave is likely to be heavily damped by collisions. As the neutral pressure is reduced (T_i increased), the mode-transformed ion Bernstein wave becomes gradually apparent. As may be seen from Fig. 10(a), the reduction in pressure causes the ion Bernstein wavelength to increase [recall that $\lambda \propto \sqrt{T_i}$ as in Eq. (11)].

To quantitatively check the mode-transformation process, we have followed the wave packet trajectory and measured the wave number as a function of the radial position. In Fig. 10(b) the measured wave number (shown as dots) is plotted as a function of the radial position in a warm-ion

plasma in which the plasma density was lowered so that the cold-plasma resonance occurs at $x \approx 2$ cm. As expected, we observe no sign of discontinuity near the resonance layer. The solid curve is obtained from Eq. (1) for $T_i = 1.5$ eV, and the dashed curve is for $T_i = 0$. The experimental data agree quite well here with theory, verifying the finite-ion-Larmor-radius mode transformation process. We note that the WKB-approximation is well satisfied throughout the experimental region.

Finally, the coherent ion Bernstein wave can provide a useful hydrogen ion temperature information in the plasma through Eq. (13) [see also Fig. 8(c)]. The ion temperature profile shown in Fig. 4(b) is obtained from the measured ion Bernstein wave dispersion relation. In Fig. 12, we also show the similarly measured ion temperature as a function of the neutral pressure. It is interesting to note that the ion temperature is roughly inversely related to the neutral pressure which is consistant with the expected ion energy loss mechanism in ACT-1, dominated by the charge-exchange and the ion-neutral collisions. This is also consistant with the previous ion temperature measurement using the electrostatic ion cyclotron wave[20] which also showed inverse-P dependence.[16]

V. Summary and Discussion

Efficient mode transformation of the electron plasma wave ($\omega \lesssim 2\Omega_i$) into an ion Bernstein wave constitutes the central element of a newly proposed method for waveguide-launched rf plasma heating. In the present experiments, this transformation has been observed in considerable detail where the measurements of $k_\perp(\omega, k_\parallel)$ and of the wave-packet trajectories have been found to be in good agreement with theory. This experimental verification of the wave excitation mechanism puts the waveguide-coupling theory[9] as well as the wave accessibility calculations[8,9] on firmer ground.

In ICRF experiments, the E_z-component of the electrostatic field near an induction coil can excite ion Bernstein waves. It is well-known that in ICRF, the induction coil is carefully Faraday-shielded to eliminate the E_z electric field. Since the fast-wave induction coil has a narrow toroidal dimension, the excited ion Bernstein wave will have a rather short $\lambda_\parallel$-spectrum which is likely to be absorbed near the plasma surface via electron Landau damping. Therefore, it is indeed prudent and necessary to shield the coil, as being practiced, to prevent such electrostatic excitation.

Finally, the excellent coherence of the externally launched ion Bernstein wave together with its strong dependence of the local hydrogen ion temperature offers an interesting T_i daignostic possibilities[23] for future fusion devices where such measurements are generally believed to become increasingly difficult. The present method can be implemented with existing microwave and/or laser scattering technology[24-26] in tokamak plasmas enabling local $\lambda_\perp$ measurement of externally launched ion Bernstein waves.

Experiments are being planned in ACT-1 to investigate possible non-linear effects associated with high-power rf on ion Bernstein wave excitation.

ACKNOWLEDGMENTS

One of the authors (M. Ono) would like to thank T. H. Stix and W. M. Hooke for helpful discussions and their continued interest in this work. Thanks are also due to J. Taylor and W. Kineyko for their valuable technical assistance.

This work was supported by the U.S. Department of Energy Contract No. DE-AC02-76-CHO3073.

REFERENCES

1. T. H. Stix, Phys. Rev. Lett. 15, 878 (1965).
2. D. G. Swanson and Y. C. Ngan, Phys. Rev. Lett. 35, 517 (1975).
3. J. Jacquinot, B. D. McVey, and J. E. Scharer, Phys. Rev. Lett. 39, 88 (1977).
4. F. W. Perkins, Nucl. Fusion 17, 1197 (1977).
5. H. Takahashi, et al., Phys. Rev. Lett. 39, 31 (1977).
6. J. Hosea, et al., Phys. Rev. Lett. 42, 1803 (1979).
7. S. Puri, Phys. Fluids 22, 1716 (1979).
8. M. Ono, Princeton Plasma Physics Laboratory Report No. 1593, 1979 (unpublished).
9. M. Ono, R. Horton, T.H. Stix, and K. L. Wong, in Proceedings of the 2nd Joint Grenoble-Varenna International Symposium of Heating in Toroidal Plasmas, (Como, Italy, 1980).
10. M. Ono and K. L. Wong, Phys. Rev. Lett. 45, 1105 (1980).
11. T. H. Stix, Theory of Plasma Waves (McGraw-Hill, New York, 1962), p. 226.
12. P. M. Bellan and M. Porkolab, Phys. Fluids, 17, 1592 (1974).
13. M. Brambilla, Plasma Physics 18, 669 (1976). (This also gives references to earlier works on mode-conversion).
14. D. G. Swanson, Phys. Fluids 10, 1531 (1975).

15. R. K. Fisher and R. W. Gould, Phys. Fluids 14, 857 (1971).

16. K. L. Wong and M. Ono, Bull. Am. Phys. Soc. 24, 957 (1979).

17. M. Ono, Phys. Rev. Lett. 42, 1267 (1979).

18. R. J. Briggs and R. W. Gould, Phys. Fluids 14, 857 (1971).

19. P. M. Bellan and M. Porkolab, Phys. Rev. Lett. 34, 124 (1975).

20. M. Ono, M. Porkolab, and R. P. H. Chang, Phys. Fluids 23, 1656 (1980).

21. J. P. M. Schmitt, Phys. Rev. Lett. 31, 982 (1973).

22. J. P. M. Schmitt and P. Krumm, Phys. Rev. Lett. 37, 753 (1976).

23. G. A. Wurden, M. Ono, K. L. Wong, and A. Semet, Bull. Am. Phys. Soc. 25, 938 (1980).

24. E. Mazzucato, Phys. Rev. Lett. 36, 792 (1976).

25. C. M. Surko and R. E. Slusher, Phys. Rev. Lett. 37, 1747 (1976).

26. W. A. Peebles, N. C. Luhmann, Jr., A. Mase, H. Park, and H. Semet, Rev. Sci. Instrum., 52, 360 (1981).

FIGURE CAPTIONS

Fig. 1. Behavior of wave dispersion relation near the lower-hybrid resonance layer (b=0). The solid curve shows mode-transformation process for $\omega \lesssim 2\Omega_i$ (a>0). The dashed curve shows mode-conversion process for $\omega >> \Omega_i$ (a<0).

Fig. 2. Mode-transformation in ACT-1 plasma. (a) Wave number vs. radial position in a hydrogen plasma with a linear rise in density. f = 12 MHz, ω/Ω_H (x=0) = 1.9, λ_n = 34 cm, n_e(b=0) = 2.5 × 10^9 cm^{-3}. (b) Wave trajectories for the case shown in (a). Wave exciter is placed at x = 0 cm.

Fig. 3. Schematic of the experimental set-up.

Fig. 4. Schematic of the tungsten filament plasma source.

Fig. 5. Radial plasma profiles in ACT-1 (a) Radial density profile (b) Electron and ion temperature profiles. Plasma center is at r = 0 cm, $P_H = 7 \times 10^{-6}$ Torr.

Fig. 6. Hydrogen ion concentration measurement by low-frequency resonance-cone propagation. (a) Radial amplitude profiles of low frequency resonance cone. Top trace is for the antenna placed three ports away and the bottom trace is

for six ports away. (b) Frequency vs measured cone angle normalized by the square root of electron-to-ion mass ratio.

Fig. 7. Radial profiles of wave amplitude for various axial positions, z(as labeled). Dashed curves are calculated trajectories. Antenna-limiter position is at x = 0 cm. The lower-hybrid resonance is at x = 1 cm.

Fig. 8. Ion Bernstein wave identification. (a) Interferometer traces. Parameters on each curve are ω/Ω_H (x=2 cm), f = 12-13 MHz, B_o(x=2 cm) = 4.2 kG, and antenna-limiter position at x = 0 cm. (b) Interferometer trace for various time delays, Δt or the phase delay in unit of 2π. Parameter on curves is $\omega\Delta t/2\pi$. (c) Wave dispersion relation. Dots are experimetal points and solid curves are the theoretical values obtained for various ion temperatures. $P_H = 7 \times 10^{-6}$Torr, $n_e \simeq 10^{10}$ cm^{-3}, x=4 cm.

Fig. 9. Ion Bernstein wave radial phase front. (a) Radial interferometry trace for various vertical positions. Antenna-limiter is at r = 5.9 cm, antenna vertical height, h = 6.3 cm. The plasma minor axis is at r = 0, h = 0, (b) Radial phase front obtained from Fig. 9(a).

Fig. 10. Mode-transformation process. (a) Radial interferometry traces for various neutral pressures. (b) Wave number vs radial position. Dots are experimental points and curves are theoretical values. Antenna-limiter is at x = 0 cm, ω/Ω_H (x=0) = 1.92, $P_H = 7 \times 10^{-6}$Torr.

Fig. 11. Ion temperature at r = 3 cm obtained from ion Bernstein wave dispersion relation vs neutral hydrogen filling pressure.

#81X0682

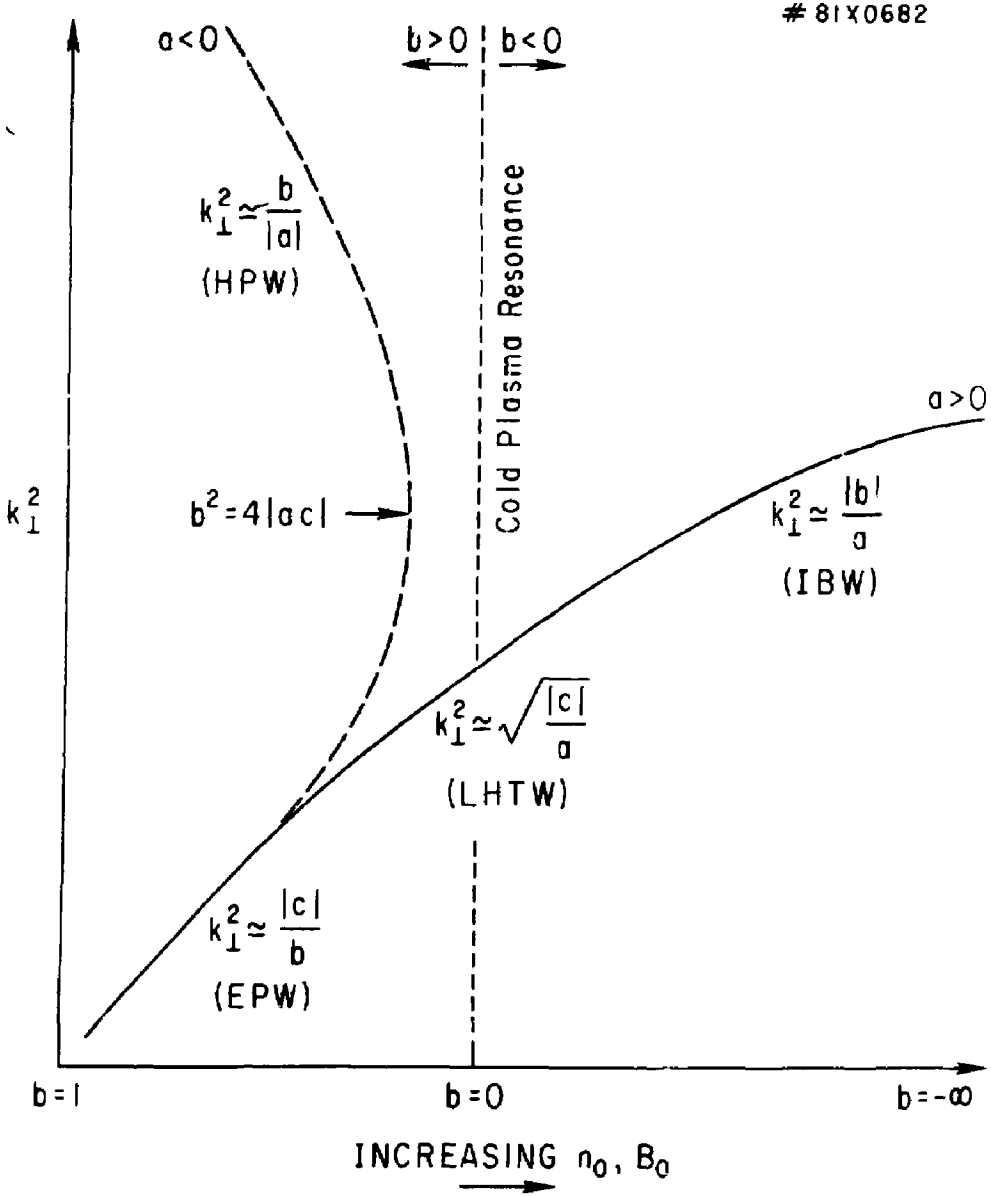

Figure 1

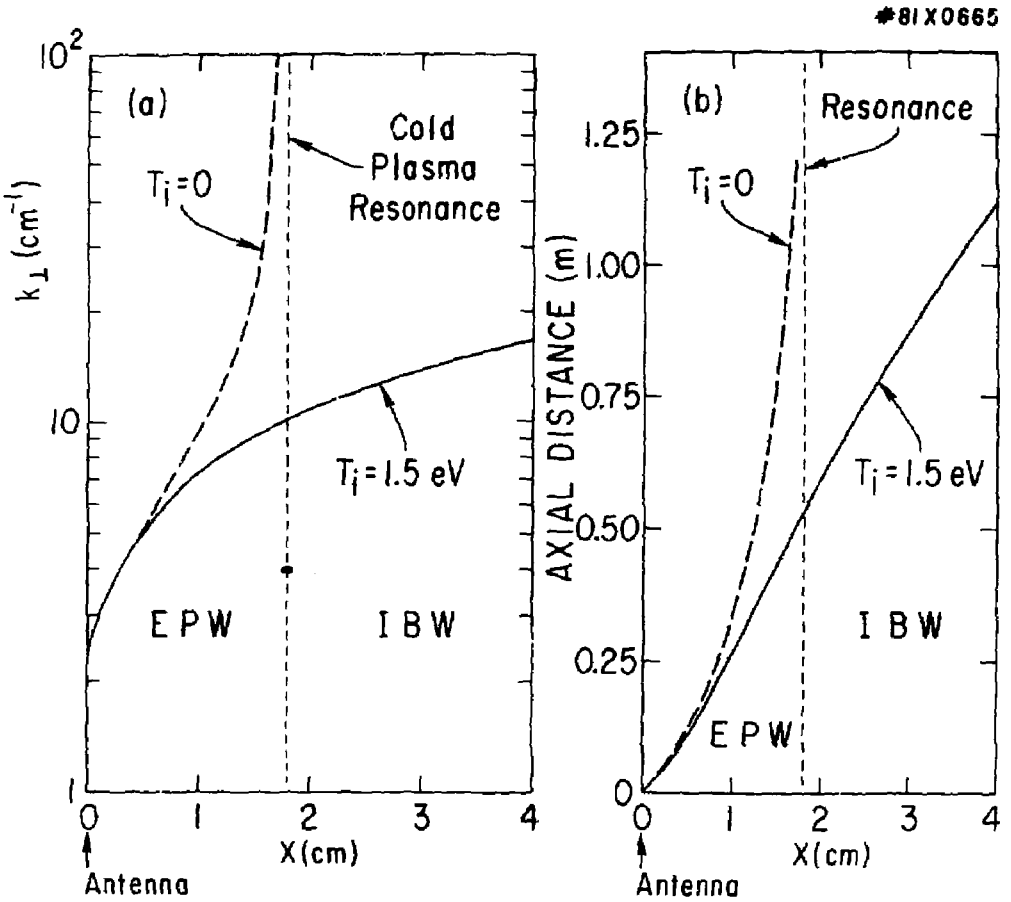
#81X0665
(a)
Cold
Plasma
Resonance
$T_i=0$
$T_i=1.5$ eV
EPW
IBW
$k_\perp$ (cm^{-1})
10^2
10
1
0
1
2
3
4
X(cm)
Antenna
(b)
Resonance
$T_i=0$
$T_i=1.5$ eV
EPW
IBW
AXIAL DISTANCE (m)
1.25
1.00
0.75
0.50
0.25
0
0
1
2
3
4
X(cm)
Antenna

Figure 2

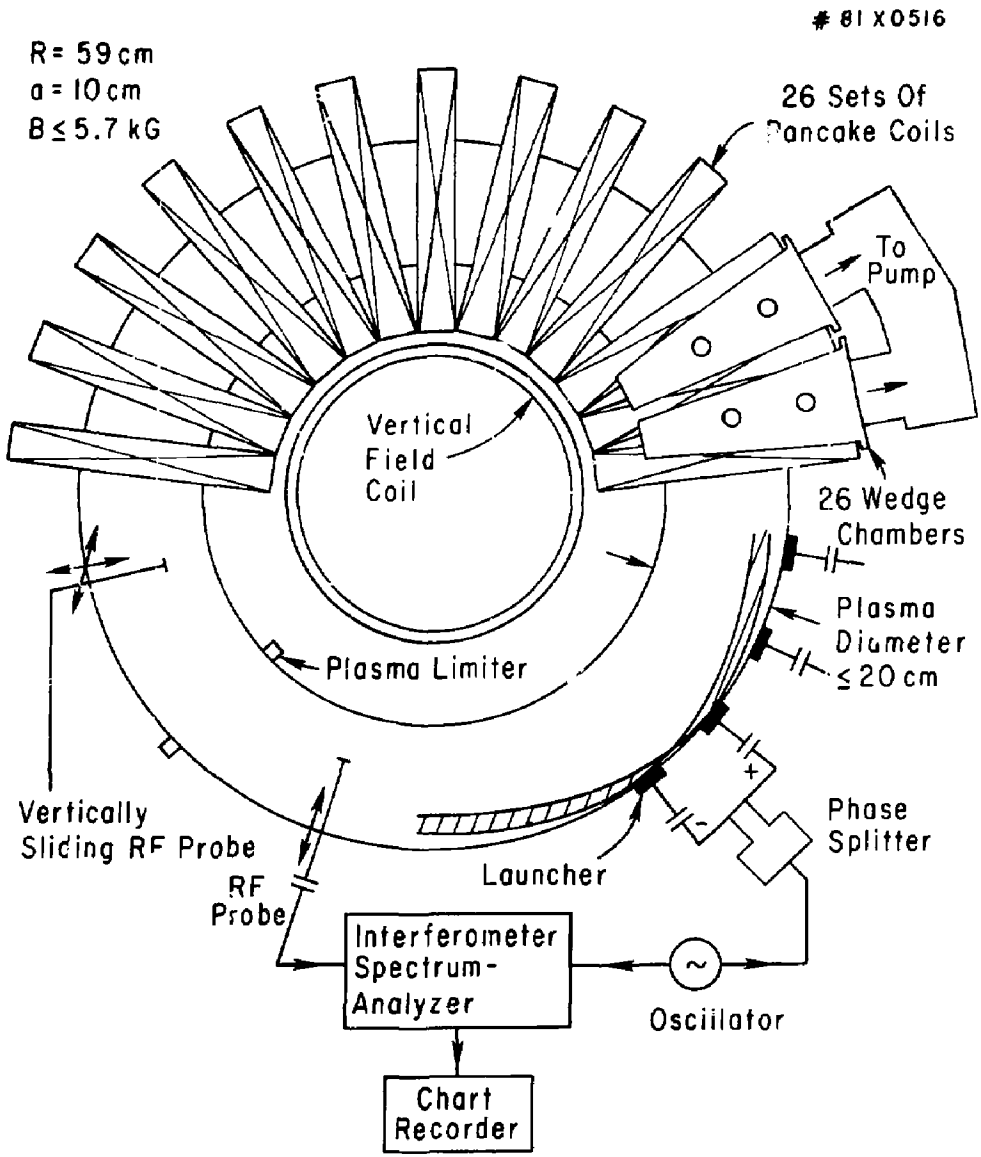
# 81 X 0516
R = 59 cm
a = 10 cm
B ≤ 5.7 kG
26 Sets Of Pancake Coils
To Pump
Vertical Field Coil
26 Wedge Chambers
Plasma Diameter ≤ 20 cm
Plasma Limiter
Vertically Sliding RF Probe
RF Probe
Launcher
Phase Splitter
Interferometer Spectrum-Analyzer
Oscillator
Chart Recorder

Figure 3

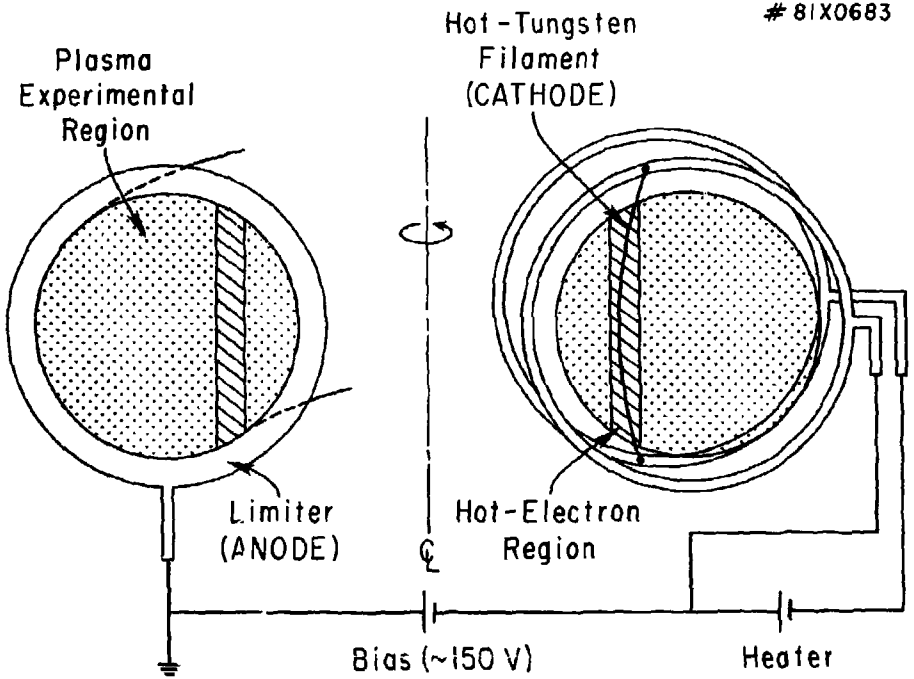
#81X0683
Hot-Tungsten
Filament
(CATHODE)
Plasma
Experimental
Region
Limiter
(ANODE)
Hot-Electron
Region
Bias (~150 V)
Heater

Figure 4

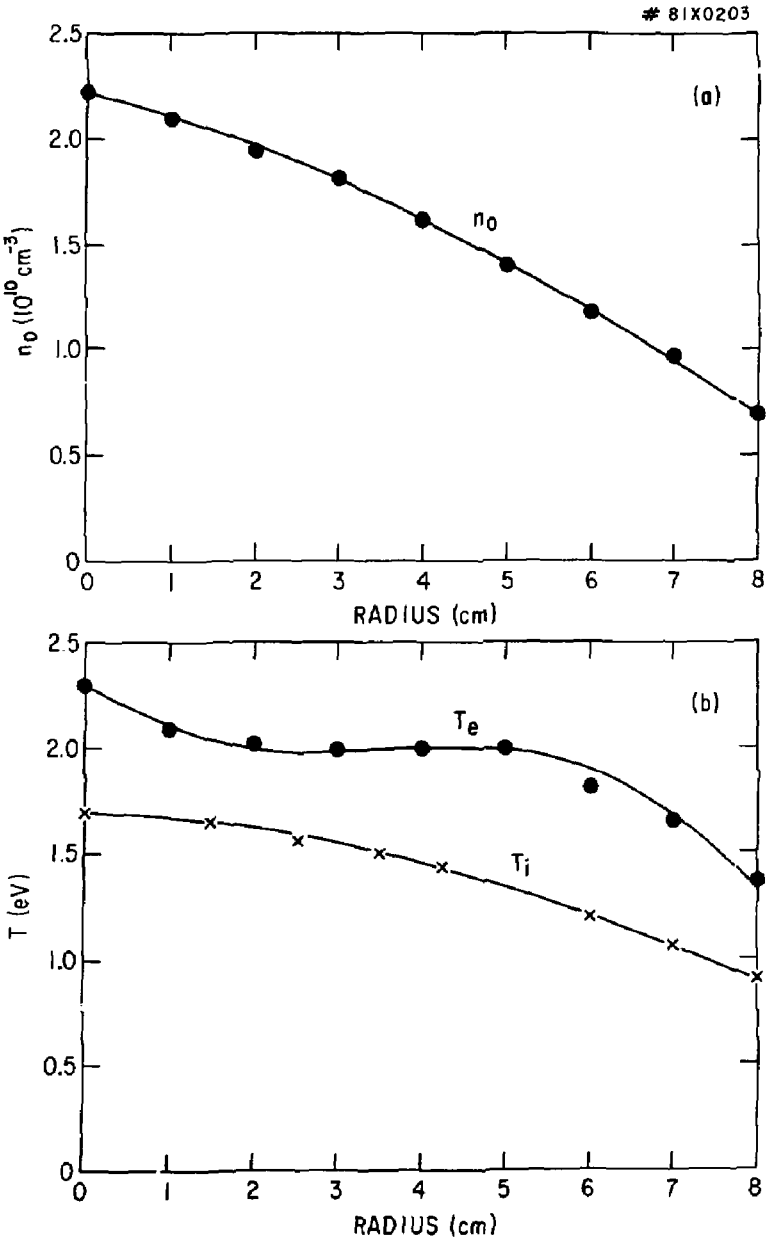

Figure 5

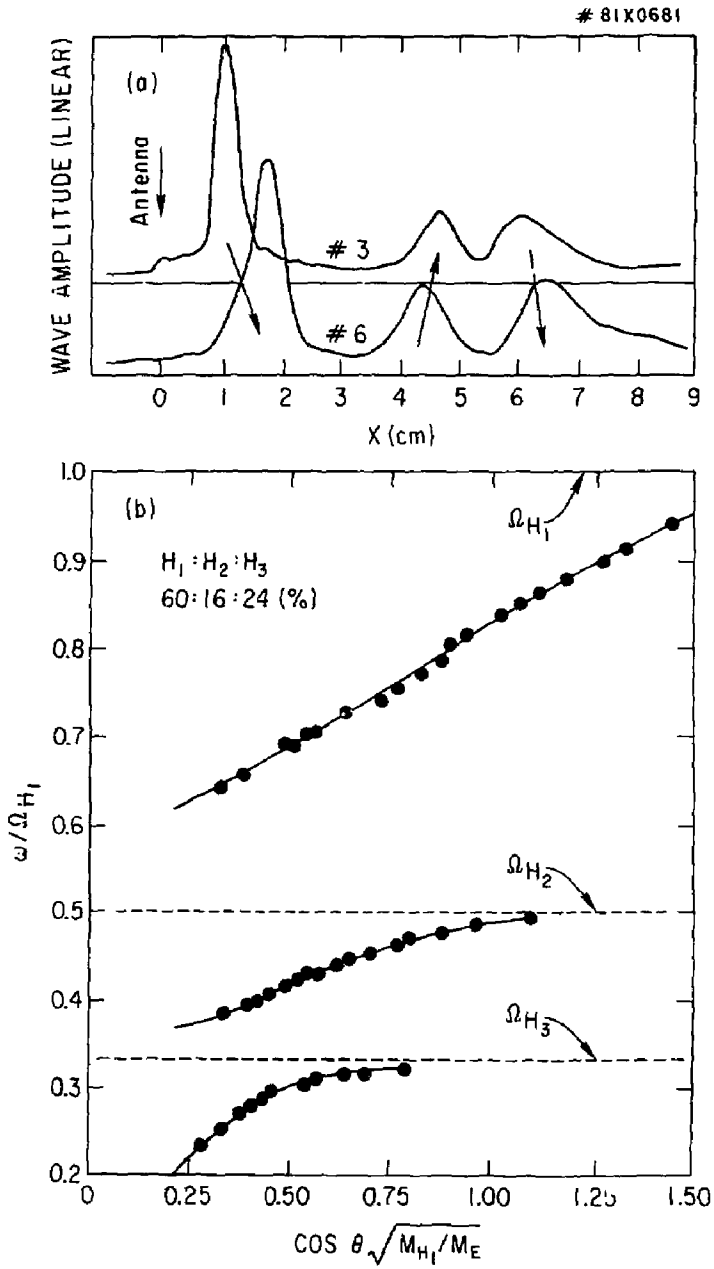
81X0681
(a)
Antenna
WAVE AMPLITUDE (LINEAR)
3
6
0 1 2 3 4 5 6 7 8 9
X (cm)
(b)
$H_1 : H_2 : H_3$
60 : 16 : 24 (%)
Ω_{H_1}
Ω_{H_2}
Ω_{H_3}
ω/Ω_{H_1}
1.0 0.9 0.8 0.7 0.6 0.5 0.4 0.3 0.2
0 0.25 0.50 0.75 1.00 1.25 1.50
COS $\theta\sqrt{M_{H_1}/M_E}$

Figure 6

#81X0662

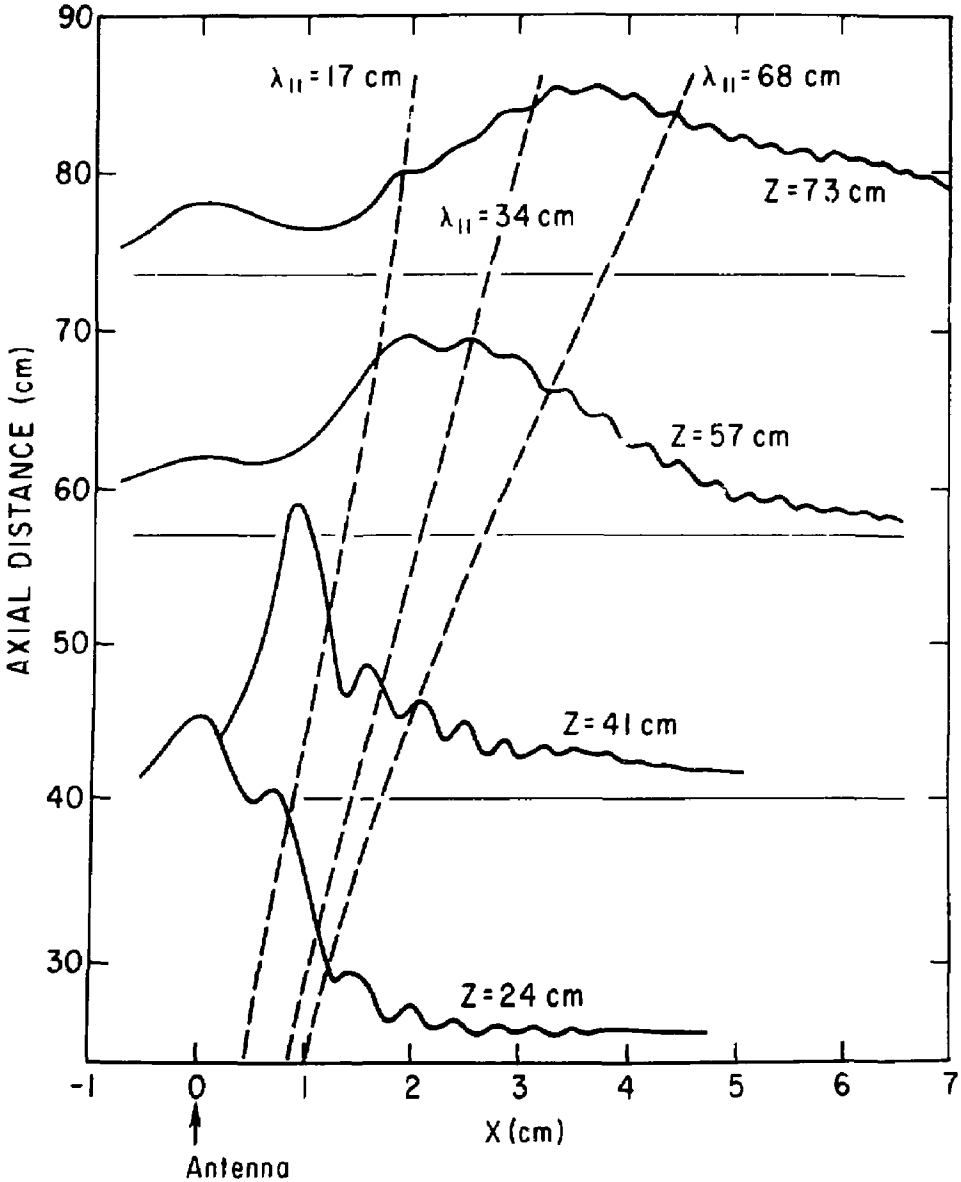

Figure 7

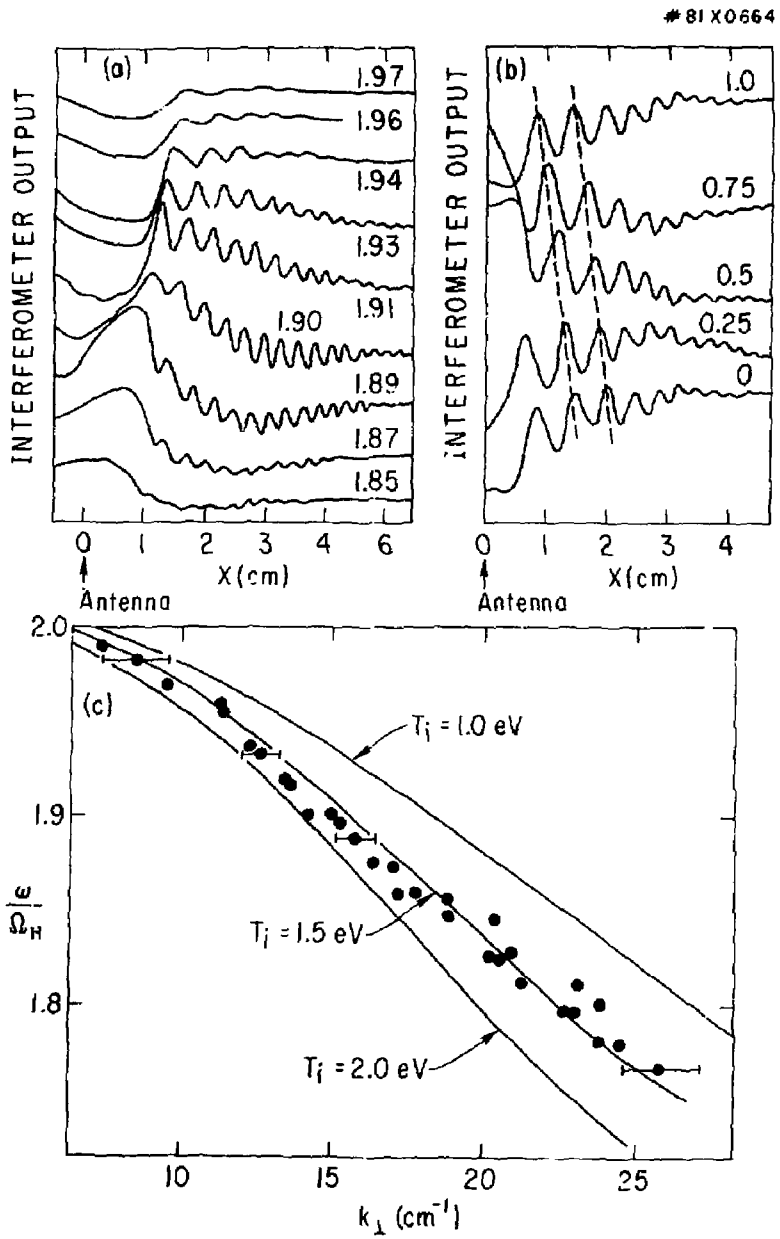
#81X0664
(a)
1.97
1.96
1.94
1.93
1.91
1.90
1.89
1.87
1.85
INTERFEROMETER OUTPUT
0 1 2 3 4 6
X(cm)
Antenna
(b)
1.0
0.75
0.5
0.25
0
INTERFEROMETER OUTPUT
0 1 2 3 4
X(cm)
Antenna
(c)
T_i = 1.0 eV
T_i = 1.5 eV
T_i = 2.0 eV
ω/Ω_H
2.0
1.9
1.8
10 15 20 25
$k_\perp$ (cm^{-1})

Figure 8

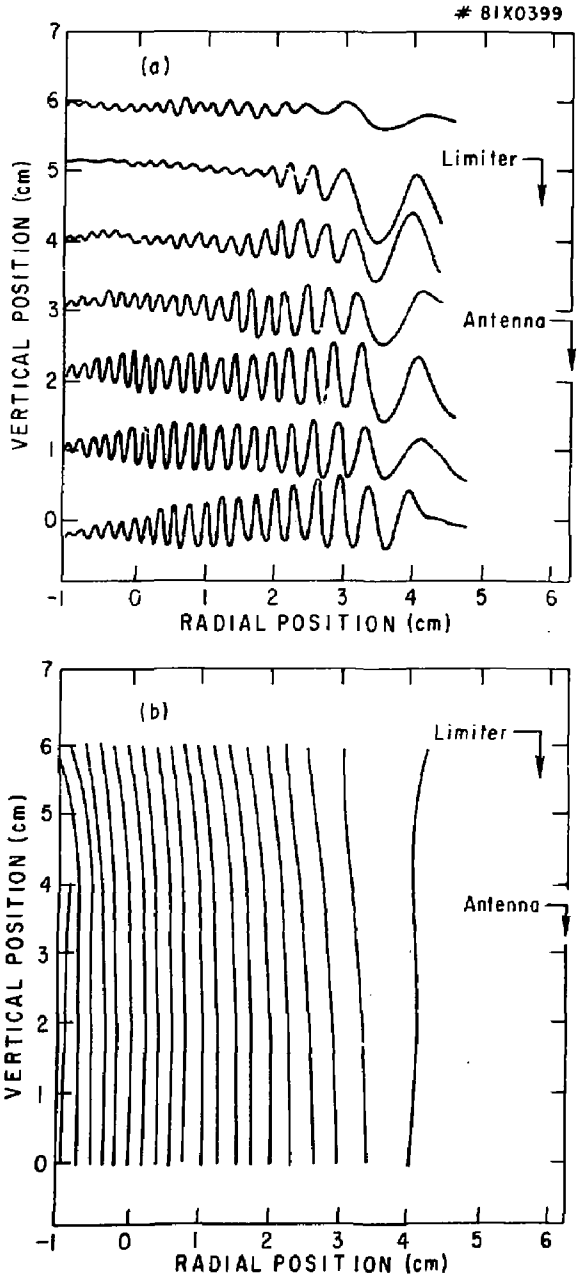
81X0399
(a)
Limiter
Antenna
VERTICAL POSITION (cm)
RADIAL POSITION (cm)
(b)
Limiter
Antenna
VERTICAL POSITION (cm)
RADIAL POSITION (cm)

Figure 9

#81X0663

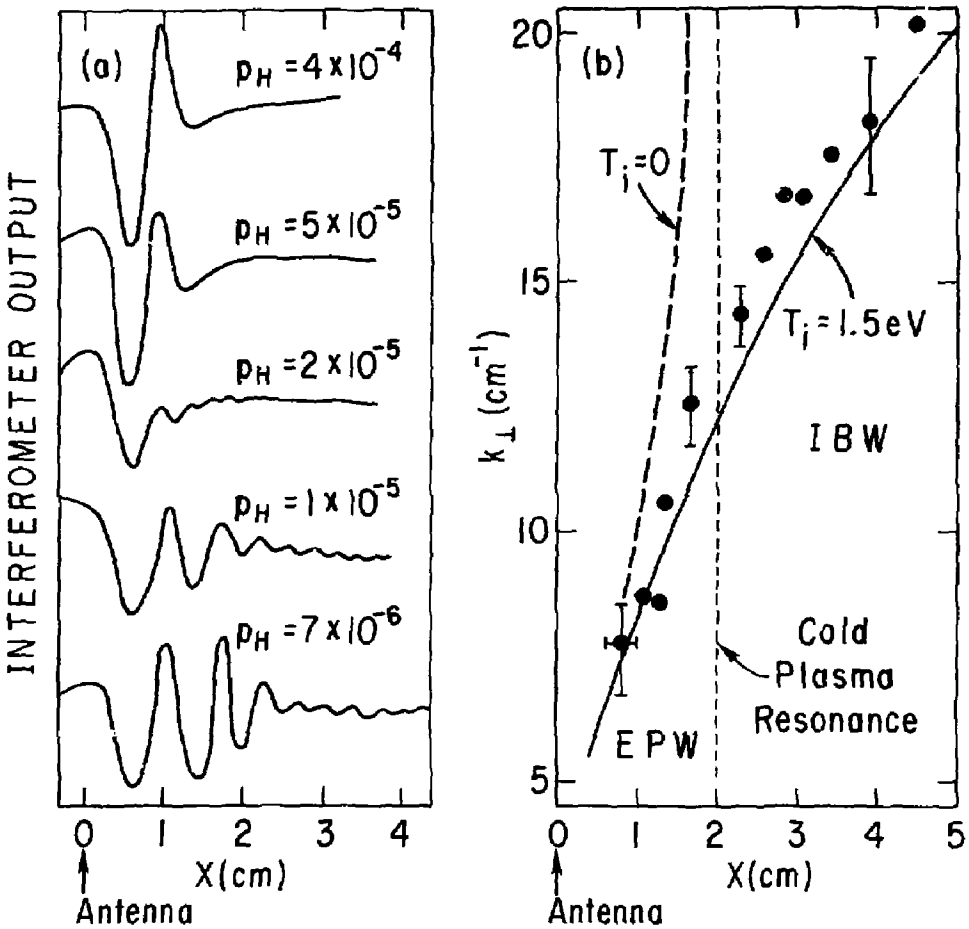

Figure 10

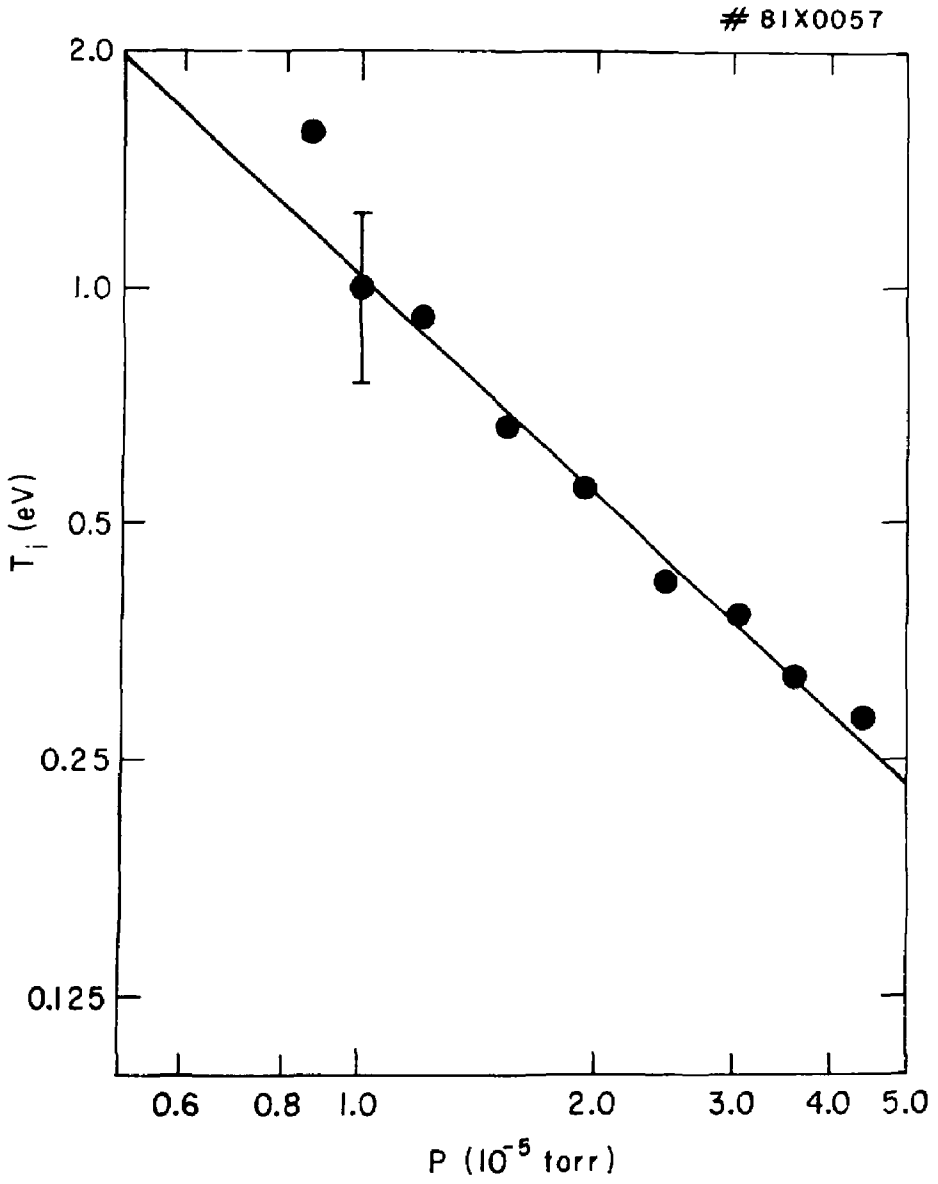

Figure 11